Particle Size Effect in Methane Activation over Supported Palladium Nanoparticles

Antje Ota[1], Edward L. Kunkes[1], Jutta Kröhnert[1], Martin Schmal[2], Malte Behrens[1,*]

[1] Fritz-Haber-Institute of the Max-Planck-Society, Department of Inorganic Chemistry, Faradayweg 4-6, 14195 Berlin, Germany

[2] Federal University of Rio de Janeiro, Programa de Engenharia Química / COPPE/NUCAT, Cidade Universitária - CP: 68502, Rio de Janeiro, RJ, 21941-972, Brasil,

*Corresponding author: behrens@fhi-berlin.mpg.de, Fax +49 (0)30 8413 4405

Abstract

A synthesis method for producing MgAl oxide supported uniform palladium nanoparticles with varying diameter has been developed. The method consists of reductive-thermal decomposition of a PdMgAl hydrotalcite-like compound, formed via co-precipitation of metal nitrate salts and sodium carbonate. The hydrotalcite–like precursors were characterized by XRD, TG-MS and SEM, and were found to contain a well defined crystalline structure and a uniform distribution of all constituent elements. The resulting catalysts were characterized by XRD, TEM, Chemisorption of CO and in-situ IR measurements of CO, and were found to consist of partially oxide-embedded Pd nanoparticles with diameters ranging from d = 1.7 to 3.3 nm and correspond dispersions of 67 to 14 %. Furthermore, the particle size was found to be inversely related to Pd loading. The palladium catalysts were studied for methane activation via chemisorption at 200 and 400 °C followed by a temperature programmed surface hydrogenation. The most disperse catalyst (d = 1.7 nm) possessed an intrinsic methane adsorption capacity, which was an order of magnitude larger than that of other catalysts in the series, indicating a strong structure sensitivity in this reaction. Additionally, the methane adsorption capacity of the hydrotalcite- derived Pd catalysts was nearly two orders of magnitude higher than that of catalysts derived through other synthesis pathways such as colloidal deposition or sonochemical reduction.

Keywords: Palladium; Hydrotalcites, co-precipitation; methane activation; non-oxidative coupling

1. Introduction

In our previous work [1] we have shown that the catalytic activity in the non-oxidative coupling of methane over Pd nanoparticles strongly depends on the preparation method and the resulting particle size. A sonochemically reduced Pd/α-Al_2O_3 catalyst and a Pd/α-Al_2O_3 sample prepared by colloidal deposition differed in particle size of Pd, widths of their particle size distributions and amount of carbon incorporation in the Pd lattice after synthesis. PdC_x was found in the colloidal sample due to carbon incorporation from the protecting ligand shell upon thermal treatment. It was shown that a large particle size has detrimental impact on the methane adsorption property and the ability to form higher hydrocarbons from methane. To further investigate the aforementioned particle size effect, in the current work we aimed at developing a synthesis concept to obtain size controlled Pd-nanoparticles and to study their catalytic performance in non-oxidative methane coupling. In our synthesis approach, hydrotalcite-like compounds (HTlc´s) are used as well-defined precursor materials, whose general formula is $[M^{2+}_{1-x}\, M^{3+}_{x}(OH)_2]\, (A^{n-})_{x/n} \cdot m\, H_2O$ [2-3] with $M^{2+} = Mg^{2+}$, Pd^{2+}, and $M^{3+} = Al^{3+}$. This synthesis concept has been previously applied for the preparation of oxide-supported intermetallic Pd_2Ga ($M^{3+} = Ga^{3+}$) nanoparticles [4]. Divalent and trivalent metal cations are incorporated in brucite-like layers and between these positively charged layers, charge-balancing anions, typically carbonate, maintain the electro-neutrality of the lattice. Furthermore the M^{2+}/M^{3+} ratio can be varied from approximately 0.2 – 0.4 to gain phase-pure materials.

Upon heating, HTlc´s decompose into mixed oxides exhibiting high specific surface area, homogeneous metal distribution, and strong interaction between the individual elements. During reduction in H_2, noble metals such as Pd segregate out of the mixed-oxide matrix to form well-define nanoparticles, whose size tends to depend on metal loading. PdMgAl hydroxycarbonates

have already been studied by several groups and were found to be active in phenol hydrogenation, oxidation of toluene, acetone condensation, hydrodechlorination of 1,2,4-trichlorobenzene and total oxidation of methane [5-9].

The catalytic methane homologation into higher hydrocarbons under non oxidative condition was proposed to be an alternative reaction to the oxidative coupling of methane, which also leads to CO_2 formation via partial combustion [10-11]. Direct conversion of methane into higher alkanes or alkenes is thermodynamically disfavored. To homologate methane it is necessary to dissociate methane by chemisorption on metal surfaces [12-14]. The adsorption and decomposition mechanism of methane on metallic surfaces is an exothermic activation process of dissociative and homolytic nature. Indeed, the kinetics of CH_4 adsorption on metallic surfaces has been studied using surface analyses, showing that atomic and electronic surface properties affect the adsorption and formation of intermediate species, and indicating that the methane dissociation is the determining step in this process [15].

The dissociation of methane on transition metals may occur directly (DDM – direct dissociative mechanism) or through a precursor mediated mechanism (PMM). In the first case the dissociation occurs during the impact at the surface while for the PMM mechanism desorption or dissociation occurs after adsorption and accommodation of the molecule at the surface. In this case, the reaction depends on the initial probability of adsorption. Most studies concluded that the DDM mechanism on transition metals is preferred [16-18]. Yang et al. [18] and Beebe et al. [19] showed that the methane dissociation on single crystal surfaces can form intermediate hydrocarbon species with one or two carbons, such as methylidene (CH), vinylidene (CCH_2) and ethylidene (CCH_3), besides graphitic carbon [20]. Lee et al. [16] observed on Ni surfaces CH fragments at very low temperatures which are recombined to C_2H_2 at temperatures

around 230 K with simultaneous desorption of H_2 at 395K. Heating favors the trimerization of the adsorbed C_2H_2 species [18].

Thus, chemisorption can lead to different carbonaceous intermediates some of which can further be hydrogenated to C_{2+} hydrocarbons. The nature and reactivity of the formed adspecies towards coupling are expected to be different dependent on the reaction conditions.[21-22] Furthermore the morphology, crystallinity, and abundance of vertices and kinks on the Pd surface may affect activity and selectivity in this reaction. For nanoparticles, these properties are closely associated with particle size, and related to the phenomenon of structure sensitivity in catalytic reactions. A straightforward correlation between single crystal surfaces and supported catalysts exists only for structure insensitive reactions, however, for structure sensitive reactions no direct correlation is possible below a certain particle size [23].

The main objective of this work is to study the influence of the particle size of nanostructured supported palladium catalysts in the activation of methane by chemisorption. Catalysts with different Pd particle sizes were prepared by co-precipitation, comprehensively characterized and their methane chemisorptions capacity was determined. The quantity and nature of methane adsorption sites was measured via adsorption followed by temperature programmed surface hydrogenation (TPSH), as outlined previously.[1] Additionally, we have compared the current results with the sonochemical and colloidal synthesis approaches reported in our earlier work [1] and the new catalysts turn out to have greater methane chemisorptions capacity. Regarding the non-oxidative coupling of methane in two steps, unfortunately no significant activity could be detected.

2. Experimental

2.1 Catalyst preparation

PdMgAl HTlc´s were synthesized by controlled co-precipitation at pH = 8.5 and a temperature of 55 °C by co-feeding appropriate amounts of mixed metal nitrate and sodium carbonate solutions. Appropriate ratio of magnesium nitrate hexahydrate ($Mg(NO_3)_2 \cdot 6\ H_2O$), aluminum nitrate ($Al(NO_3)_3 \cdot 4\ H_2O$) and palladium nitrate solution ($Pd(NO_3)_2 \cdot 2\ H_2O$) were mixed with deionized water. The Pd:Mg:Al atomic ratio was x:70-x:30 (x = 0.1, 0.5, 1.0, 1.5 and 2.5). A 0.345 M sodium carbonate solution was used as precipitating agent. Both solutions were added simultaneously dropwise into a 2L precipitation reactor (Mettler-Toledo LabMax). After completion of addition, the mixture was kept for ageing at 55 °C and with stirring for 1 h. The precipitate was filtered and washed two times with warm deionized water in order to remove the nitrate and sodium ions. The solid was dried for 12 hours at 80 °C in air. The precursor was reduced in 5% H_2 in Argon at 500 °C. A heating rate of 2 °C/min was chosen to achieve a mild reduction procedure after which the temperature was kept constant for 240 min. Precursor samples will be hereafter referred to as Pd*x*, where x is the 10× nominal Pd content in mol-%. A sample with a Pd loading of 0.1 mol-% is for instance labeled Pd01.

2.2. Catalyst characterization

X-ray diffraction (XRD) patterns of the HTlc precursor and its decomposition products were recorded on a STOE Stadi P diffractometer in transmission geometry using a primary Ge monochromater, Cu $K\alpha_1$ radiation and a 3° linear position sensitive detector. Specific surface areas (SSA) of the precursors and reduced compounds were determined by N_2 adsorption–desorption measurements at 77 K by employing the BET method (Autosorb-1C, Quantachrome). Prior to N_2 adsorption, the sample was outgassed at 80 °C (precursors) / 150°C (reduced

samples) to desorb moisture from the surface and pores. Thermogravimetric analysis (TGA) was performed on a Netzsch STA449 thermobalance. The reduction process was studied in 5 vol% H_2 in Argon up to temperatures of 800 °C (2 °C/min). Inductively coupled plasma optical emission spectrometry (ICO-OES) was used for chemical analysis. Known amounts of the sample were dissolved in aqua regia and the content of the metals is determined after matrix matched calibration on a Vista RL, Varian. Scanning electron microscopy (SEM) images were acquired with a Hitachi S4800 FEG microscope equipped with an EDS system (EDAX) for elemental analysis. The samples were loosely dispersed on a conductive carbon tape to preserve the as-prepared morphology as much as possible. EDX spectra were acquired at an accelerating voltage of 15 kV. Transmission electron microscopy (TEM) images of Pd nanoparticles were acquired using a FEI TITAN microscope, equipped with a field emission gun (FEG) and operated at 300 kV. With computer assisted correction and alignment, the value of the spherical aberration constant C_s was kept below 100 nm in the present experiments. Typically, several scanning TEM (STEM) images of different regions were imaged for analysis of the particle size. Volumetric CO chemisorption measurements were carried out in an Autosorb 1C (Quantachrome Instruments). The samples were pretreated in situ in the sample cell by heating to 500 °C for 60 min in 5 % H_2 in argon flow (20 ml/min), followed by an evacuation (120 min) at pretreatment temperature. The samples were cooled down to 40 °C under vacuum and the chemisorption measurement was performed in the pressure range of 2-560 torr. The active surface area can be determined by using the Dual isotherm method. The weak isotherm curve was measured after the combined isothermal curve and contains only the physisorbed part of the CO because all adsorption sites for the chemisorbed CO are still occupied. The difference of combined and weak

isotherms results in the chemisorbed amount of the CO. The metal surface area, dispersion and particle size was calculated according [24].

The infrared (IR) spectroscopy of adsorbed CO was carried out using a Perkin-Elmer Pe100 spectrometer equipped with a MCI detector. The spectra were recorded with a resolution of 2 cm^{-1} and an accumulation of 64 scans. Self-supported wafers were obtained by pressing the powdery sample under a pressure of 123 MPa. The sample was treated directly in the IR cell which is connected to a vacuum system with a residual pressure of about 10^{-7} mbar. Prior the CO adsorption measurements, the samples were reduced in 500 mbar H_2 at 500 °C for 2 h and then evacuated at the same temperature for 30 min. The empty cell was used to generate background spectra. Difference spectra were obtained through substraction of the spectrum of the treated sample in vacuum from the spectrum in presence of CO.

2.3. Methane adsorption

In a temperature programmed surface hydrogenation (TPSH) experiment, a sample of 100-350 mg of catalyst was reduced in 5 % H_2 in He (50 ml/min) at 500 °C for 30 minutes in a quartz glass microreactor. Then, the sample was swept with He flow to remove H_2 traces on the metal surface and cooled down to RT in the same atmosphere. After 30 min the catalyst was heated to the chemisorption temperature (200° or 400 °C). After temperature stabilization methane was admitted for 1 min at a flow rate of 300 ml/min and then the sample rapidly cooled down in methane to room temperature within 6 min to avoid ageing of the chemisorbed species. Weakly adsorbed methane was removed by a high He flow (300 ml/min) for 30 min. In the subsequent surface hydrogenation step pure H_2 with a flow of 50 ml/min was admitted and the reactor was heated with 20 °C/min up to 500 °C. To achieve complete removal of the carbonaceous deposits

the catalyst was kept at this temperature for 1h. Mass signals related to methane (m/e = 15), ethane (m/e = 30), ethylene (m/e = 28), propane (m/e = 43) and propylene (m/e = 41) were monitored. A reference experiment with a Pd-free MgAl HTlc-derived catalyst did not show any measurable methane adsorption capacity under these conditions in the absence of Pd particles.

3. Results and discussion

3.1 Catalyst preparation and characterization

We have used a ternary HTl precursor consisting of Pd^{2+}, Mg^{2+} and Al^{3+} and carbonate as interlayer anions. Mg^{2+} was partially substituted by Pd^{2+} and the Pd content was varied from 0 – 2.5 mol-% of all metal species in order to obtain different Pd particle sizes in the final catalysts. The Al^{3+} content was constant at 30 mol-% to obtain phase-pure HTlc's. The precursor materials were prepared by controlled co-precipitation and thermally reduced in hydrogen at 500 °C. Table 1 presents an overview of all prepared samples. In total, 6 samples were synthesized with different Pd loading ranging from 0 to 8 wt-% in the final catalyst. There are deviations between the nominal and the measured composition in particular for the Al content, which varies from 30 to 39 mol-%. The Pd content, however, is in good agreement with the nominal values and no other precursor phases except for the HTlc could be observed (vide infra). The specific surface area (BET) of the co-precipitated HTlc precursors, determined by N_2 physisorption, decreased with increasing Pd content from 191 to 84 m²/g, while no changes of the pore structure have been observed (Figure S 2). In contrast, no correlation between palladium content and surface area could be found for the thermally reduced samples and the surface area of the Pd/$MgAlO_x$ catalysts varied from 196 to 242 m²/g.

XRD revealed that all precursor samples crystallize in hydrotalcite-like structure as shown in Figure 1. The reflexes are relatively broad indicating low crystallinity and/or small crystallite size. It is noted that the peaks are slightly shifted to higher angles because of the increased Al^{3+} content in comparison to MgAl hydroxycarbonate reference pattern (ICDD 14-191). The lattice parameter *a* and *c* for Pd doped precursor samples do not show a clear trend with Pd content. The *a* parameter of the Pd-containing samples are basically identical to the Pd free MgAl-HTl sample with exception of the sample richest in Pd. This suggests that the substitution of Mg^{2+} by Pd^{2+} has only little impact on the structure, although Pd^{2+} exhibits a larger ionic radius. No Pd containing byphase was observed by XRD up to a Pd loading of 2.5 mol-%.

Scanning electron microscopy was applied to study the morphological properties of the materials. As shown in Figure 2, typical plate-like particles were obtained for all the samples. The thickness of the platelets is in the low nanometer range, while the lateral dimension is approximately around 250 nm or below. The EDX line scan of the Mg K-, Al K- and Pd L-fluorescence lines revealed a homogenous metal distribution of all three cations (Figure 2). Pd seems to be well distributed and no agglomerates could be identified by SEM.

To study the transformation of the HTlc precursor into the $Pd/MgAlO_x$ catalyst upon heating in reducing atmosphere, TGA measurements have been performed in hydrogen-containing atmosphere. The weight loss profile and the corresponding MS signals are shown in Figure 3. The two stages below 150 °C involved desorption of surface-bound and interlamellar water. Simultaneously CO_2 from weakly bound carbonate ions was released in small quantities. At temperatures above 200 °C two additional weight loss steps occurred. This stage has been ascribed to the partial dehydroxylation of the brucite like layers and decarbonation of the interlayer. By further temperature increase, CH_4 is observed in addition to H_2O. This is a first

indication that Pd particles have formed in the material. At sufficiently high temperature, CO_2 resulting from the carbonate decomposition of the HTl precursor is instantaneously hydrogenated to CH_4 by gas phase hydrogen on the metallic Pd surface.

X-ray diffraction patterns of reductively treated samples do hardly show evidence of Pd metal, because the particles are too small and the amount of Pd is too low to give sharp XRD peaks (Figure 4). Only a broad modulation of the most intense (111) line of metallic Pd is observed at $2\theta \approx 40°$ for the samples with high Pd loadings. The other XRD peaks of the reduced sample can be identified as MgO. The Al-phase is amorphous and no peaks corresponding to Al_2O_3 or $MgAl_2O_4$ are detected in the XRD patterns. TEM and CO chemisorption measurements were performed to estimate the dispersion and size of the metallic particles.

After reductive treatment, the material has preserved the platelet-like morphology of the HTlc precursor and small spherical particles were formed, as presented in the micrograph in Figure 5A for Pd25 catalyst. HAADF-STEM micrographs were used to determine the particles size distribution. The good contrast between the metallic particles (white spots in Figure 5B) and the $MgO/MgAl_2O_4$ support allowed for measuring of individual particles. It can be clearly seen that the particles are well dispersed and below 5 nm in size. Particles even smaller than 1 nm are also present. HRTEM images (Figure 5C) show the presence of small Pd metal particles on the surface of the disordered oxide support. The support was identified as MgO and nanocrystalline $MgAl_2O_4$ by analysis of the lattice fringes observed in the oxide matrix (not shown). In case of the Pd01 catalyst no particles could be found because of the low Pd loading and small size. The resulting Pd particle size distributions of the other samples are shown in Figure 6. While the sample with a Pd loading of 1.49 wt-% exhibits an average size of 1.9 nm and a narrow size distribution, increasing the Pd content to 8 wt-% shifts the maximum to higher particle sizes to

3.3 nm and results in an a broader distribution. The average particles sizes of ≤ 3.5 nm are quite small considering the thermal treatment at 500 °C. Thus, some control over the particle size distribution of Pd is possible using the HTlc precursor approach for the preparation of supported Pd nanoparticles. The more the Pd^{2+} ions are diluted in the precursor lattice, the smaller the resulting Pd metal particles are after thermal reduction. At higher Pd loadings between 4 and 8 wt-%, no further growth of the Pd particles was observed. This is probably due to a limit of Pd^{2+} incorporation into the HTl cationic lattice between 1.5 and 2.5 mol-% Pd. For compositions beyond this limit, extra-lattice Pd species would be formed in the precursor material, which should form a small amount of larger aggregates not detected with high resolution electron microscopy.

In comparison to TEM, which measures particle size directly, chemisorption measures the adsorbed gas amount on the accessible metal surface. Uptakes of irreversibly absorbed carbon monoxide were determined by the dual isotherm method to discriminate between reversible and irreversible adsorbed species. CO can be chemisorbed dissociatively (CO:Pd ≥ 2) or associatively in a linear (n = 1), bridged (n = 2) and capped (n = 3) form.[25] Due to the proportion of linear to bridged carbonyl species obtained during CO infrared adsorption (vide infra, Figure 7), a CO:Pd stoichiometry of 1.5 were chosen to calculate dispersion and particle size in agreement with the British Standard.[26] Dispersion between 14 and 25 % and particle sizes ranging from 4.5 to 8.2 nm were obtained for all catalysts above 1 wt-% Pd loading by this method. Only the Pd01 catalyst is an exception. It showed about a much higher dispersion (67 %) and a much smaller particle size (1.7 nm). When comparing the chemisorption data with the particles sizes determined by HAADF-STEM micrographs, the slight size overestimation by volumetric measurements becomes evident. Apparently CO does not have complete access to the

metallic Pd surface, probably due to the synthesis approach, which results in strong embedding of particles. The initially perfect atomic distribution of Pd^{2+} in the precursor leads to a strong interfacial contact of Pd metal particles and the oxide matrix upon thermal reduction. Under this assumption, the embedding of the nanoaprticles can be calculated by comparison of TEM and chemisorptions data. While for Pd05 embedding of 78% of the nanoparticle's surface was observed, it decreases to 64% for Pd content > 1 mol%, see Table 2.

Adsorption of CO on Pd nanoparticles was studied for selected catalysts with IR spectroscopy at room temperature by exposing samples with CO pressures up to 50 mbar. Before the measurements the catalysts were re-reduced in the setup to clean the metallic surface. Corresponding IR spectra of 0.1 mol% and 1.5 mol-% Pd sample [1] at a CO pressure of 1 mbar are shown in Figure 7. The spectra show characteristic bands in the carbonyl region of 2100-2000 cm^{-1} and 1970-1700 cm^{-1}. These bands are typical for linearly and bridged-bonded CO on Pd^0 surfaces, respectively.[27] The first band at 2077 cm^{-1}can be assigned to CO linearly bonded on Pd^0, while the band at lower wavenumber is characteristic for two-fold coordinated CO. According to Lear at al. [28] this band at 1960 cm^{-1} can be assigned to bridged-bonded CO on Pd(110) facets and particles edges. For Pd01 the band of on-top coordinated CO is more intense than that of bridged-bonded CO and can be attributed to small particle size, high dispersion and reflect the heterogeneity of the surface termination of the Pd crystallites.[29] With higher Pd loading the amount of bridged-bonded CO adsorbate is increased due to bigger particles with larger facets and lower dispersions. These observations are in a good agreement with the particles size trend observed by TEM.

In summary, a series of $Pd/MgO/MgAl_2O_4$ catalysts have been prepared and characterized. They are comprised of Pd nanoparticles, which form during the thermal reduction of the PdMgAl HTlc

precursor in hydrogen. These particles are thermally stable up to 500 °C and their size can be controlled to some extent between < 1.9 and 3.5 nm by adjusting the Pd content during synthesis. The sample with the lowest Pd loading of 0.33 wt-% shows a much higher Pd dispersion compared to those samples with Pd contents between 1.5 and 8 wt-%.

3.2 Methane adsorption

The kinetics of CH_4 adsorption on metallic surfaces have been studied by TPSH. Lin et al. [30] studied methane chemisorption and conversion on metallic surfaces and calculated the dissociation energy of C-H bonds of methane. They showed that the main dissociated species is CH_3, because it has the highest energetic barrier to split further bondings in the reaction $CH_3 \rightarrow CH_2 + H$ on all surfaces. The higher the adsorption strength the higher is the energy necessary to move surface species that migrate over the surface to meet other fragments for reacting. Coupling of CH_3 can form ethane and they concluded that ethylene should be formed through dehydrogenation of ethane and not by non-oxidative coupling reactions. Ciobica et al. [31] calculated that on Ru (1120) the most stable species is CH_2^* and that the intermediate CH_x ($1 < x < 3$) are more stable when adsorbed on bridged sites, while C species are preferentially adsorbed on top sites. The effect of particle size was studied by Ma et al. [32] for Pt nanoparticles supported on zeolites, who observed higher formation of C_2+ products with increasing particle size. Belgued et al. [21, 33] and Martins et al. [34] observed high conversions at low temperatures during the chemisorption step of methane on different catalysts assuming the formation of surface carbides after methane decomposition of methane at higher temperatures and subsequently hydrogenation at lower temperatures with the formation of alkanes, according to Koerts et al. [11, 14].

In fact, during methane adsorption different types of surface carbonaceous intermediates can be generated on metallic Pd surface. In literature mainly three kinds of species are distinguished on the basis of desorption temperature during TPSH [14, 35-37]:

C_α: - Carbidic surface carbon with the best yield of carbon-carbon bond formation upon hydrogenation (T < 100 °C). At very low carbon coverages these species can undergo a reversible transformation to C_β

C_β: - Amorphous, mostly unreactive carbon. Reacts to form methane (T ~ 200 °C) and is irreversibly transformed into Cγ in an ageing process

C_γ: - Unreactive, graphitic carbon reacts to form methane and no other products (T > 400 °C)

In Figure 8 the methane evolution during hydrogenation of the surface carbonaceous intermediates after the adsorption of methane at 200 °C on our catalysts are presented. Only minor amounts of other hydrocarbon species, in particular very small amounts of ethane as the only coupling product, have been detected in the effluent gas of all experiments. The contribution of carbidic carbon (C_α) is comparatively low and cannot be sufficiently separated from the amorphous carbon (C_β). Thus, the low amount of coupling products produced over our catalysts is probably related to the inability of the Pd particles to form the carbidic C_α species under these conditions. Main carbon species resulting from the decomposition of methane are C_β and C_γ. $C_ß$ consists of two components, one at 200 °C ($C_{\beta1}$) and a second at 350 °C ($C_{\beta2}$). The hydrogenation of C_γ slowly starts at 450 °C and stops in the isothermal regime at 500 °C. The profiles of all catalysts showed certain trends. With increasing Pd content there was an increase in the amount of amorphous carbon, whereas the amount of the graphitic carbon was not influenced significantly with exception of catalyst Pd01. While at low loadings the high

temperature peak ($C_{\beta 2}$) of the amorphous carbon dominates the methane capacity per gram catalyst, the low temperature peak ($C_{\beta 1}$) had a higher contribution at high Pd loading. The ratio of $C_{\beta 1}$ to $C_{\beta 2}$ changes from 1:2 for Pd05 to 2:1 for Pd25. As already mentioned Pd01 is an exception and shows a much higher capacity in the formation of carbonaceous deposits. Pd01 exhibited a $C_{\beta 2}$ content of 72 µmoles CH_4 per gram catalyst, the highest value for all catalysts tested, as shown in Table 3. The amount of graphitic carbon amount was six times higher than the highest value obtained for Pd15 of 6 µmoles CH_4 per gram catalyst, while the total amount of carbonaceous deposits was comparable with that of catalyst Pd15.

By normalizing the total amount of desorbed methane by the Pd content, the high specific capacity of the low Pd loading catalyst Pd01 became more apparent, as shown in Figure 9. While the capacities of the sample Pd05 – Pd25 are similar between 2.8 and 2.1 mmoles CH_4 per gram Pd (in the order Pd10 < Pd25 < Pd15 ~ Pd05), that of Pd01 was higher by an order of magnitude and amounts to 36.6 mmoles CH_4 per gram Pd.For the adsorption experiments at 400 °C, a fresh specimen was used and pretreated under the same conditions as catalyst for the 200 °C measurements. After methane exposure and flushing in Helium the carbonaceous adspecies were hydrogenated. At first glance, the profiles appeared similar to those measured at 200 °C (see Figure 10). There is a negligible amount of C_α and the main products are amorphous (C_β) and graphitic carbon (C_γ). The C_β species consists, as in the 200 °C experiment, of a low and a high temperature contribution for both of which an increase was noted with increasing Pd loading. Furthermore, the peak maxima of these contributions are shifted closer together. For all catalysts the major contribution to the methane capacity is the $C_{\beta 2}$ species, as presented in Figure 10. As observed in the 200 °C experiment, the catalyst Pd01 deviated again and showed a higher activity, comparably high to the Pd15 catalyst. Normalization of the total amount of methane

formed per gram Pd result in the following capacity series: Pd25 (3.5 mmol) < Pd15 (3.8 mmol) ≈ Pd10 (3.8 mmol) < Pd05 (5.2 mmol) << Pd01 (46.1 mmol). Again, sample Pd01 is 13 times more active than the catalyst which possesses the highest Pd loading.

The correlations of the adsorption capacity of methane at 200° and 400 °C with the catalyst amount and the Pd content are summarized in Figure 11. Firstly, the methane adsorption capacities of the catalysts rose with increasing adsorption temperature. An increase between 20 % and 52 % was observed. Secondly, the amount of methane per gram catalyst increases with Pd content in an approximately linear fashion for each adsorption temperature except for catalyst Pd01. Its activity is similar to that of the catalyst with twelve times higher Pd content (Pd15). The exceptional methane capacity of this sample is even more obvious if the amount of desorbed methane is normalized by the Pd loading. The by far highest capacity was observed for the Pd01 catalyst, while all other catalysts show similar values.

These observations suggest that the significantly higher dispersion and therefore smaller particle size of Pd01 compared to other catalysts in the series, results in an enhancement of the intrinsic methane activation capacity (Figure 12). The existence of a particle size effect in Pd nanoparticles for the methane adsorption capacity indicates that this adsorption is highly structure sensitive. This effect is present only below a certain critical size, of ~2 nm. Above this critical size the total methane activation capacity scales nearly linearly with the Pd loading, while the intrinsic capacity remains approximately independent of Pd loading.

Thus, through lowering the Pd loading, catalysts with average particle sizes of < 1.9 to 3.3 nm can be synthesized, and within this small range of particle sizes, the intrinsic methane adsorption capacity varies by an order of magnitude. One likely explanation for the observed structure sensitivity may be the higher density of coordinatively unsaturated Pd atoms present in the

highly dispersed Pd01 catalyst. Such unsaturated sites bind dissociation products stronger and therefore provide a greater driving force for methane activation. Cortright et al. [38] have shown through DFT calculations that dehydrogenated hydrocarbon species and their transition states interact stronger with the Pt(211) stepped surfaces as compared with close packed Pt(111). To that end, Klier et at. [39] have studied the methane activation (C-H cleavage) on Pd single crystals and have found that stepped open surfaces such as Pd(679) are an order of magnitude more active than close-packed surfaces such as Pd(111). Goodman [40] has observed a similar trend with ethane hydrogenolysis on Ni surfaces. Our results provide yet another example of how structure sensitivity plays an important role in hydrocarbon activation.

Comparison of the methane adsorption capacities reported here to those measured on Pd/Al_2O_3 catalysts prepared by sonochemical reduction (200 °C: 0.9, 400 °C: 8.1 $\mu mol/g_{cat}$) and colloidal deposition (200 °C: 5.7, 400 °C: 23.1 $\mu mol/g_{cat}$) reveals considerably higher values for the co-precipitated samples [1]. This is probably a result of the higher dispersion and smaller particles that could be achieved with this method. The particle size obtained by colloidal and sonochemical preparation were 10 and 6 nm in average, respectively, while co-precipitated samples exhibit particles sizes smaller than 5 nm.

In addition to the investigation of the influence of particle size and methane adsorption temperature, the recyclability and stability of catalysts prepared by co- precipitation were tested using Pd15 as an example. To that end, three consecutive TPSH experiments were performed and the results are presented in Figure 13. First a standard TPSH experiment was performed with the reduction step at the beginning, adsorption at 400 °C and a subsequent hydrogenation up to 500 °C for 1h time on stream. This procedure was repeated again and the corresponding profile labeled TPSH2. TPSH3 included an oxidative treatment at 500 °C (10 °/min, 30 min holding

time) in 20% O_2 in Helium (50ml/min) followed by same reduction as for TPSH 1 and 2. During oxidation, no oxidized carbon in form of CO and CO_2 was observed. For all TPSH experiments the same profiles were observed and quantitatively the same amount of amorphous and graphitic carbon was formed on the metallic Pd particles indicating that the catalysts were stable in this temperature range and that hydrogenation has removed all surface carbon species.

In summary, it could be shown that a particle size effect exists for methane activation on very small Pd clusters of a size below 2 nm. These particles displayed a significantly higher intrinsic methane adsorption capacity than others in the series, whose intrinsic capacity seems comparable. The thermal stability of the co-precipitated catalysts was found to be excellent as exemplified for a sample with intermediate particle size.

4. Conclusions

A synthesis method for supported Pd catalysts was presented, which allows a certain control over the particle size by variation of the Pd substitution in the cationic lattice of the HTlc precursor material. A series of catalysts with Pd loadings between 0.3 and 8 wt-% has been prepared and the resulting $Pd/MgO/MgAl_2O_4$ catalysts exhibit a homogenous microstructure, high specific surface area, a relatively uniform particle size distribution and average Pd particle sizes between < 1.9 and 3.5 nm, which is thermally stable up to temperatures as high as 500 °C. The methane adsorption capacity of these catalysts was generally very high compared to Pd samples prepared by other methods. In particular, an extraordinary high capacity was observed for the sample with the lowest loading. This observation indicates the existence of a size effect in Pd nanoparticles for the adsorption of methane. A critical Pd cluster size below 1.9 nm is required for the enhanced adsorption to take place.

Acknowledgements

The authors thank Frank Girgsdies for help with XRD pattern refinement, Gisela Weinberg for SEM investigations, Dirk Rosenthal for the help with the CO chemisorption measurement, and Nigel Hamilton for the IR experiments, Norbert Pfänder and Wei Zhang for recording the TEM images and Igor Kasatkin for the HRTEM analysis. Robert Schlögl is acknowledged for valuable discussions and continuous support. Furthermore, the authors would like to thank Fabio S. Toniolo, Maria Auxiliadora S. Baldanza, Antônio José de Almeida and Rodrigo Brackmann for their substantial assistance and support during the measurements in the NUCAT/COPPE laboratories. This project was supported by the Deutsche Forschungsgemeinschaft (444 BRA-113/67/0-1) and CNPq (490788/2008-4). -34

References

[1] S.F. Moya, R.L. Martins, A. Ota, E.L. Kunkes, M. Behrens, M. Schmal, Appl. Catal. A:Gen. 411-412 (2012) 105-113.

[2] A. De Roy, Mol. Cryst. Liq. Cryst. Sci. Technol. A:Mol. Cryst. Liq .Cryst. 311 (1998) 173 -193.

[3] C. Forano, T. Hibino, F. Leroux, C. Taviot-Gueho, in: F. Bergaya, B.K.G. Theng, G. Lagaly (Eds.), Handbook of Clay Science, Elsevier, 2006, pp. 1021-1095.

[4] A. Ota, M. Armbrüster, M. Behrens, D. Rosenthal, M. Friedrich, I. Kasatkin, F. Girgsdies, W. Zhang, R. Wagner, R. Schlögl, J. Phys. Chem. C. 115 (2010) 1368-1374.

[5] S. Narayanan, K. Krishna, Appl. Catal. A:Gen. 174 (1998) 221-229.

[6] J. Carpentier, J.F. Lamonier, S. Siffert, E.A. Zhilinskaya, A. Aboukaïs, Appl. Catal. A:Gen. 234 (2002) 91-101.

[7] A.A. Nikolopoulos, B.W.L. Jang, J.J. Spivey, Appl. Catal. A:Gen. 296 (2005) 128-136.

[8] F. Basile, G. Fornasari, M. Gazzano, A. Vaccari, Appl. Clay Sci. 18 (2001) 51-57.

[9] B.T. Meshesha, R.J. Chimentão, A.M. Segarra, J. Llorca, F. Medina, B. Coq, J.E. Sueiras, Appl. Catal. B:Enviro. 105 (2011) 361-372.

[10] M. Belgued, P. Pareja, A. Amariglio, H. Amariglio, Nature. 352 (1991) 789-790.

[11] T. Koerts, R.A. van Santen, J. Chem. Soc. Chem. Commun. (1991) 1281-1283.

[12] A. Amariglio, M. Belgued, P. Paréja, H. Amariglio, J Catal. 177 (1998) 113-120.

[13] H. Amariglio, M. Belgued, P. Paréja, A. Amariglio, J Catal. 177 (1998) 121-128.

[14] T. Koerts, R.A. van Santen, J. Mol. Catal. A:Chem. 74 (1992) 185-191.

[15] J. Szanyi, D.W. Goodman, Rev Sci Instrum. 64 (1993) 2350-2352.

[16] M.B. Lee, Q.Y. Yang, S.T. Ceyer, J Chem Phys. 87 (1987) 2724-2741.

[17] M. Valden, J. Pere, N. Xiang, M. Pessa, Chem Phys Lett. 257 (1996) 289-296.

[18] Q.Y. Yang, A.D. Johnson, K.J. Maynard, S.T. Ceyer, J Am Chem Soc. 111 (1989) 8748-8749.

[19] T.P. Beebe, D.W. Goodman, B.D. Kay, J.T. Yates, J Chem Phys. 87 (1987) 2305-2315.

[20] T.V. Choudhary, D.W. Goodman, Top Catal. 20 (2002) 35-42.

[21] M. Belgued, A. Amariglio, P. Paréja, H. Amariglio, J. Catal. 159 (1996) 441-448.

[22] P. Pareja, S. Molina, A. Amariglio, H. Amariglio, Appl. Catal. A:Gen. 168 (1998) 289-305.

[23] D.W. Goodman, J Phys Chem-Us. 100 (1996) 13090-13102.

[24] G. Ertl, H. Knözinger, F. Schüth, J. Weitkamp, Handbook of Heterogeneous Catalysis, 2nd ed., Wiley-VCH Verlag GmbH & Co. KGaA, 2008.

[25] J.J.F. Scholten, A.P. Pijpers, A.M.L. Hustings, Catal. Rev. Sci Eng. 27 (1985) 151 - 206.

[26] B. Standard, Determination of the Specific Surface Area of Powders. Recommendations for Methods of Determination of Metal Surface Area Using Gas Adsorption Techniques., 1995.

[27] N. Sheppard, C. De La Cruz, Catal. Today. 70 (2001) 3-13.

[28] T. Lear, R. Marshall, J.A. Lopez-Sanchez, S.D. Jackson, T.M. Klapotke, M. Baumer, G. Rupprechter, H.-J. Freund, D. Lennon, J. Chem. Phys. 123 (2005) 174706-174713.

[29] S. Bertarione, D. Scarano, A. Zecchina, V. Johanek, J. Hoffmann, S. Schauermann, J. Libuda, G. Rupprechter, H.J. Freund, J Catal. 223 (2004) 64-73.

[30] Y.Z. Lin, J. Sun, J. Yi, J.D. Lin, H.B. Chen, D.W. Liao, J Mol Struc-Theochem. 587 (2002) 63-71.

[31] I.M. Ciobica, R.A. van Santen, J. Phys. Chem. B. 106 (2002) 6200-6205.

[32] J.H. Ma, S.H. Reng, D.H. Pan, R.F. Li, K.C. Xie, React Funct Polym. 62 (2005) 31-39.

[33] M. Belgued, A. Amariglio, P. Pareja, H. Amariglio, J. Catal.. 159 (1996) 441-448.

[34] R.L. Martins, M.A. Baldanza, M.M.V.M. Souza, M. Schmal, Stud Surf Sci Catal. 147 (2004) 643-648.

[35] D.W. Goodman, R.D. Kelley, T.E. Madey, J.T. Yates Jr, J. Catal. 63 (1980) 226-234.

[36] T.M. Duncan, J.A. Reimer, P. Winslow, A.T. Bell, J. Catal. 95 (1985) 305-308.

[37] T.M. Duncan, P. Winslow, A.T. Bell, J. Catal. 93 (1985) 1-22.

[38] R.D. Cortright, R.M. Watwe, J.A. Dumesic, J. Mol. Catal. A:Chem. 163 (2000) 91-103.

[39] K. Klier, J.S. Hess, R.G. Herman, J. Chem. Phys. 107 (1997) 4033-4043.

[40] D.W. Goodman, Surf Sci. 123 (1982) L679-L685.

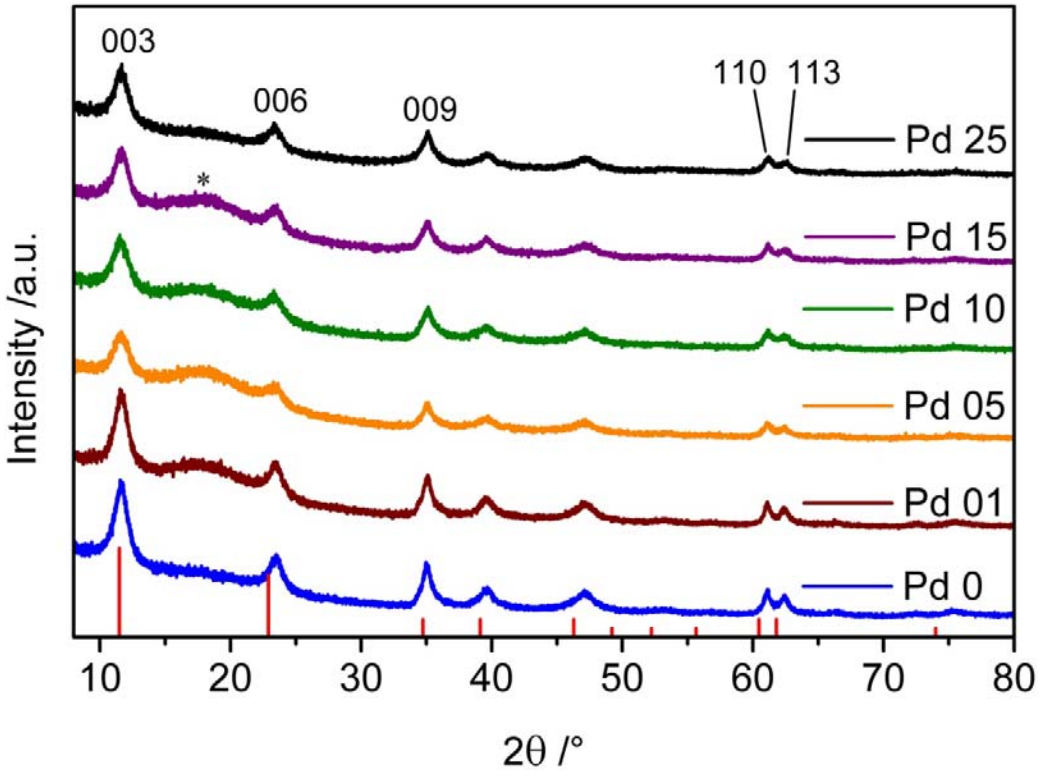

Figure 1: X-ray diffraction pattern of PdMgAl HTl compounds with different Pd loadings (red lines: $Mg_6Al_2(OH)_{16}CO_3 \cdot 4\ H_2O$ (ICDD 14-191); * grease).

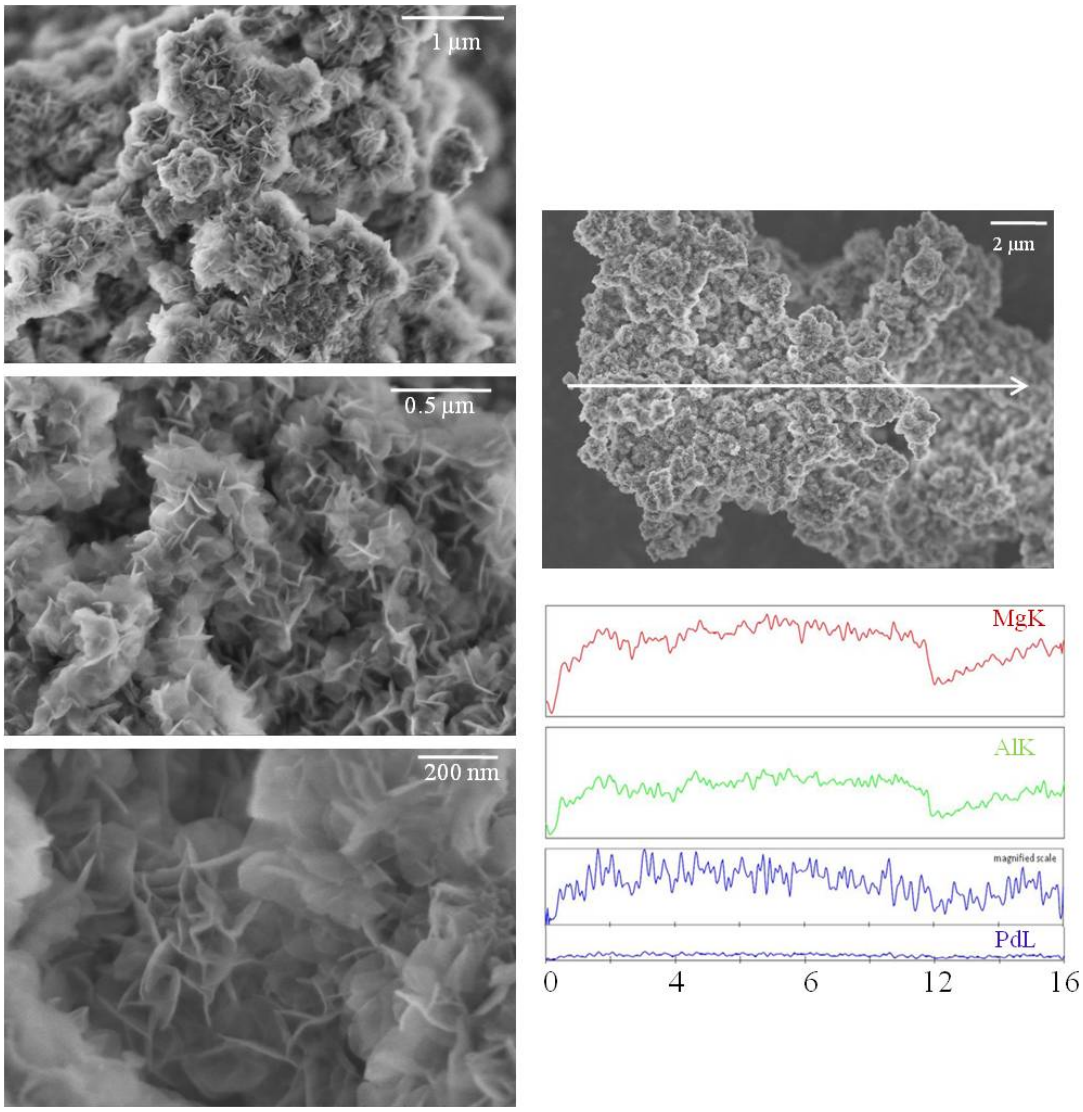

Figure 2: Typical morphology of the PdMgAl precursor and EDX line scan to illustrate the metal distribution (Pd15 shown).

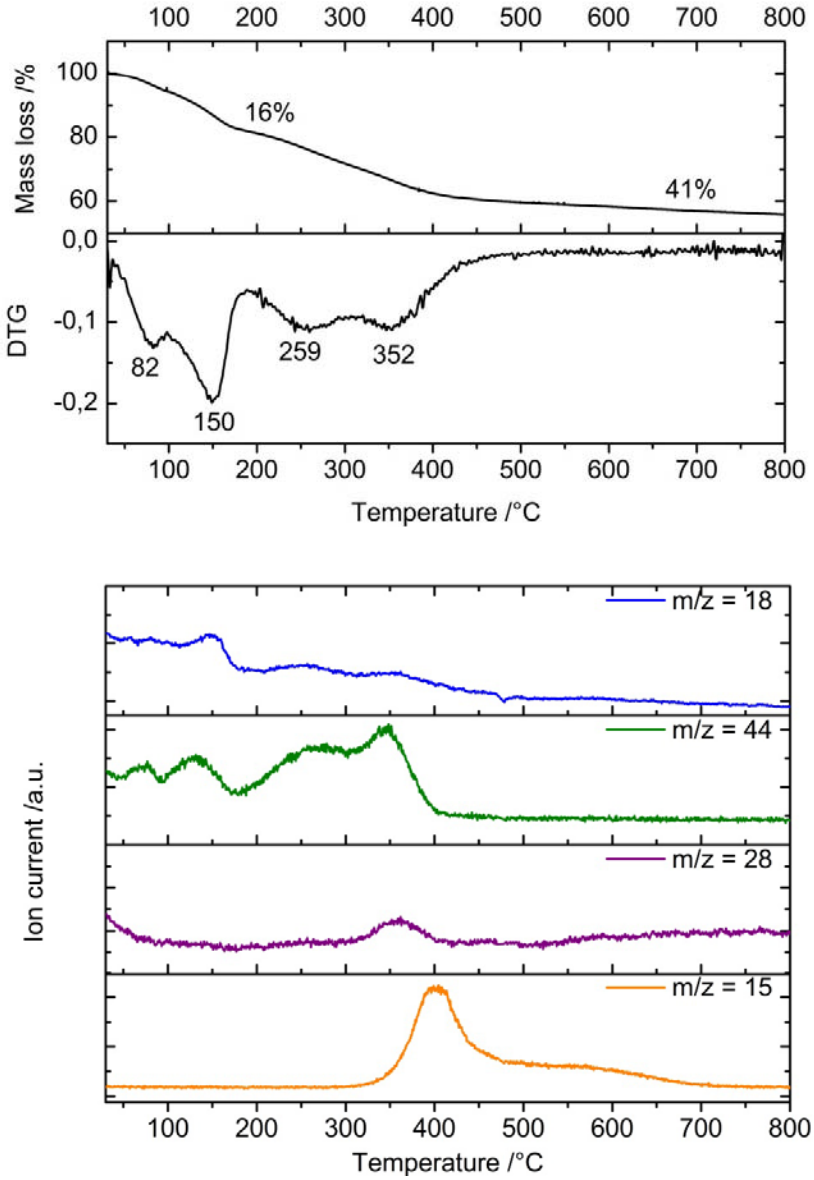

Figure 3: TG-MS data of precursor Pd15 in 5% H_2 in Argon (2Kpm).

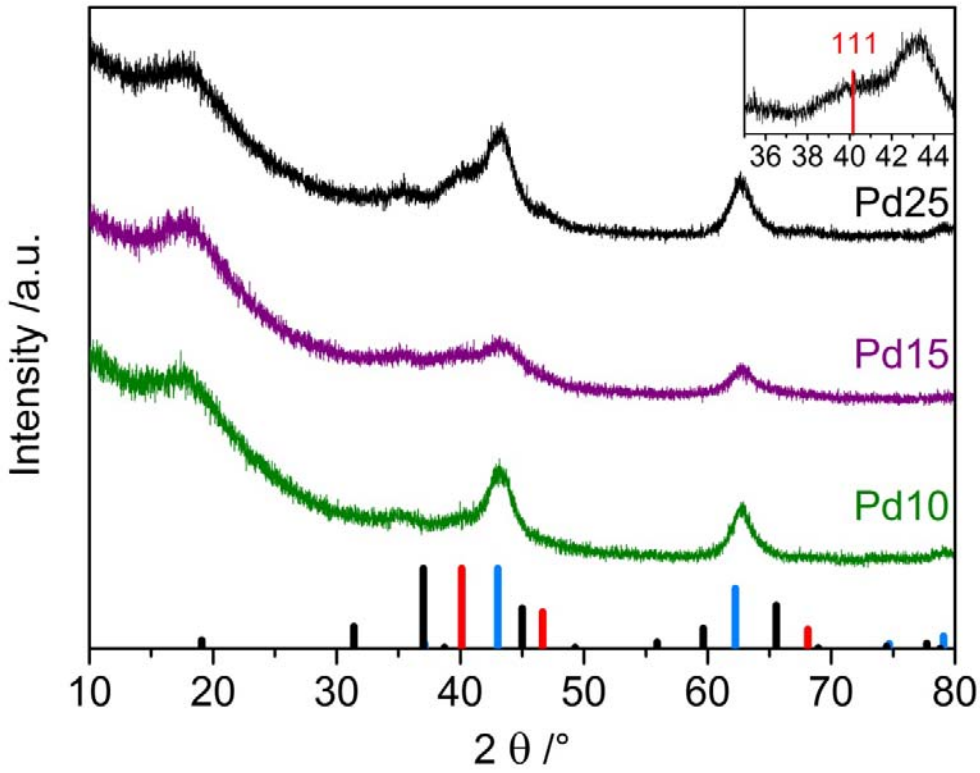

Figure 4: XRD pattern of Pd10, Pd15 and Pd25 after reduction at 500 °C. Red lines correspond to metallic Pd (ICDD 01-1439), blue lines to MgO (ICDD 01-1235), and black lines to $MgAl_2O_4$ (ICDD 73-1959).

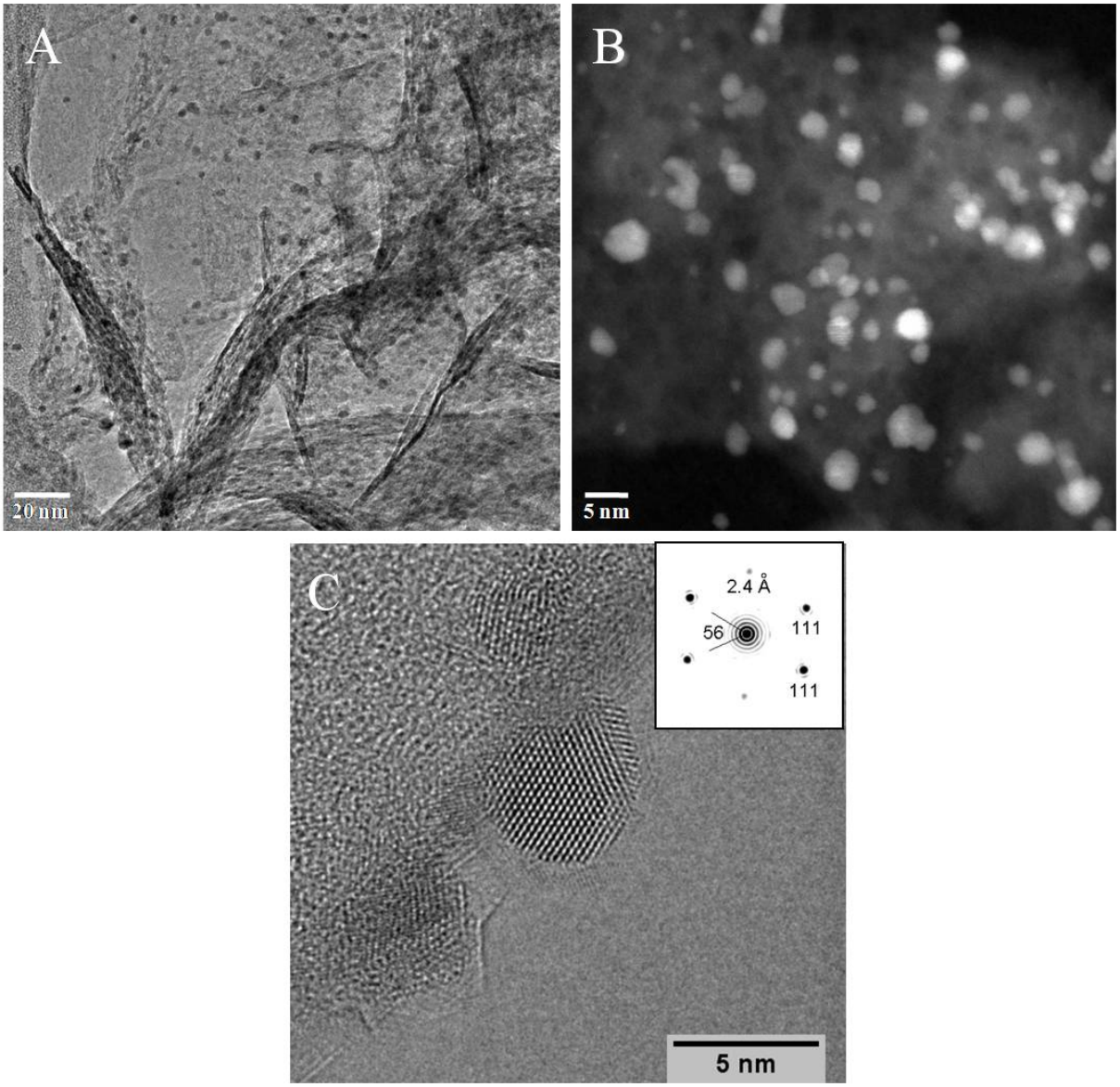

Figure 5: (A) Overview micrograph, and (B) HAADF-STEM of Pd nanoparticles supported on $MgO/MgAl_2O_4$ (Pd25) (C) HRTEM of twinned Pd particle along (111) plane (boundary along image plane). The upper and lower spots in PS correspond to "imaginary" distance of 2.4 Å due to interference.

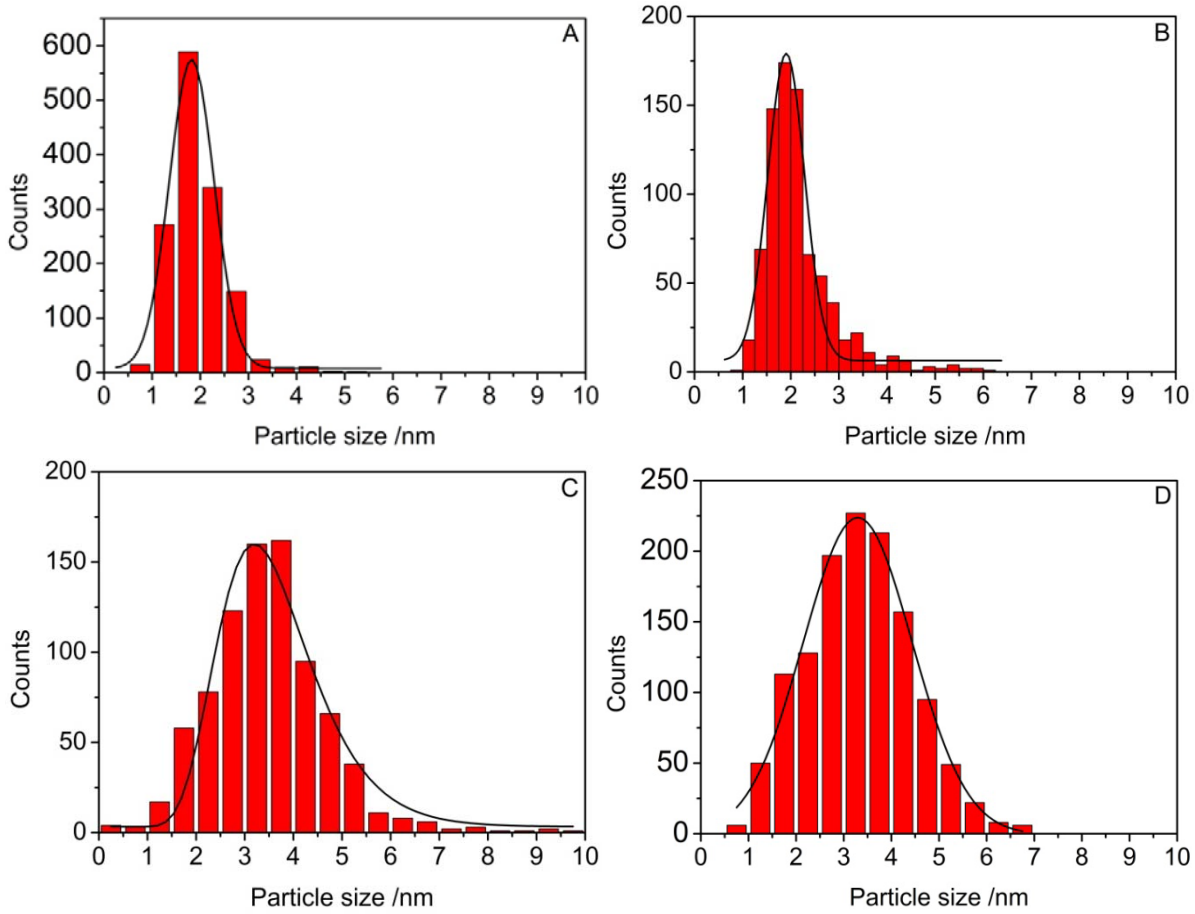

Figure 6: Particle size distribution of Pd05 (A), Pd10 (B), Pd15 (C) and Pd25 (D) from TEM images.

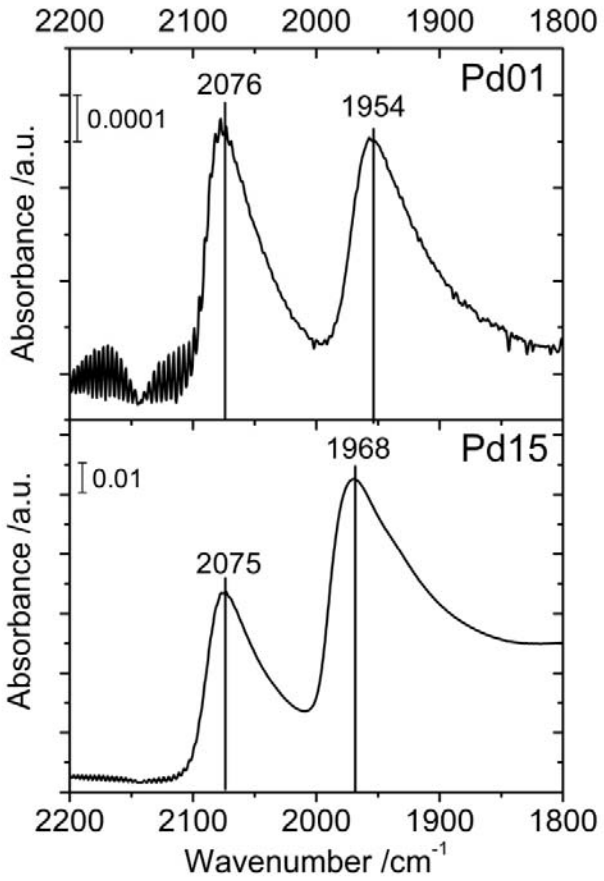

Figure 7: CO-IR spectra of Pd01 and Pd15 after reduction at 500 °C in the CO stretching region from 2200 to 1800 cm^{-1} at CO pressure of 1 mbar (room temperature).

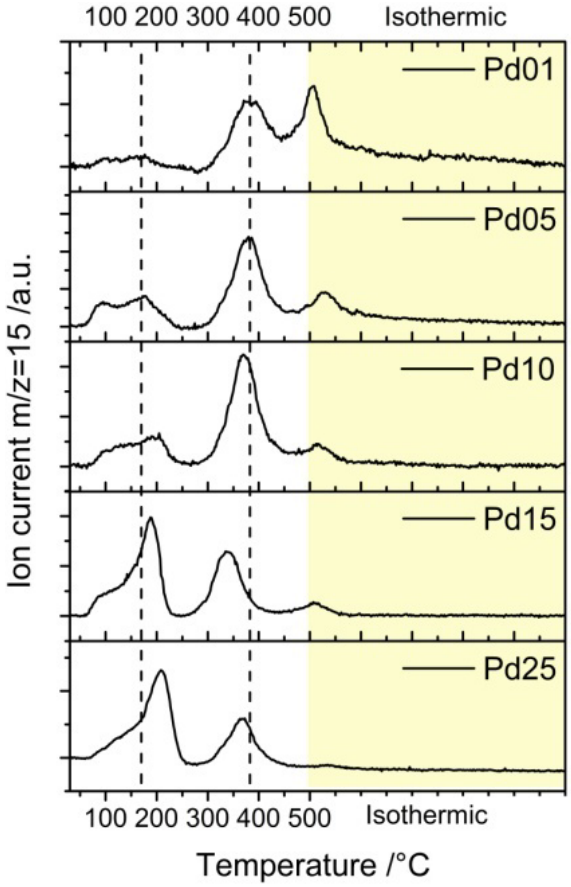

Figure 8: Methane profiles of temperature-programmed hydrogenation of surface carbonaceous intermediates after methane adsorption at 200 °C.

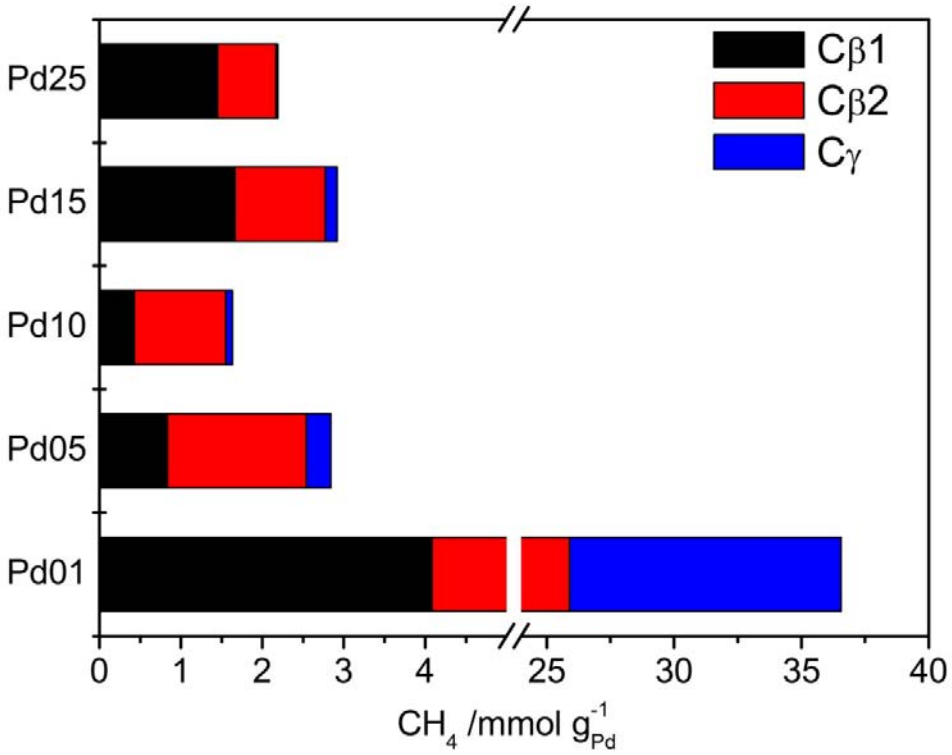

Figure 9: Methane capacity per gram Pd after adsorption at 200 °C.

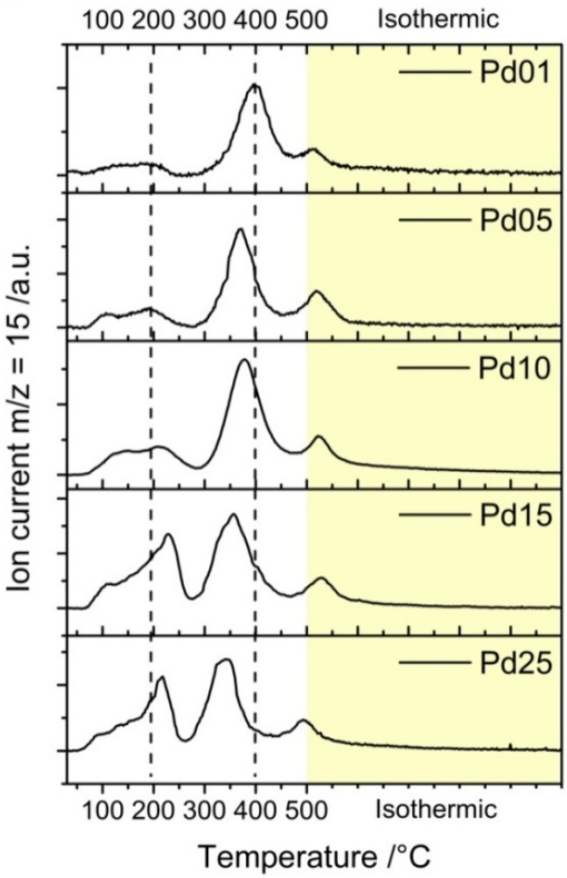

Figure 10: Profiles of temperature-programmed hydrogenation of surface carbonaceous intermediates after methane adsorption at 400 °C.

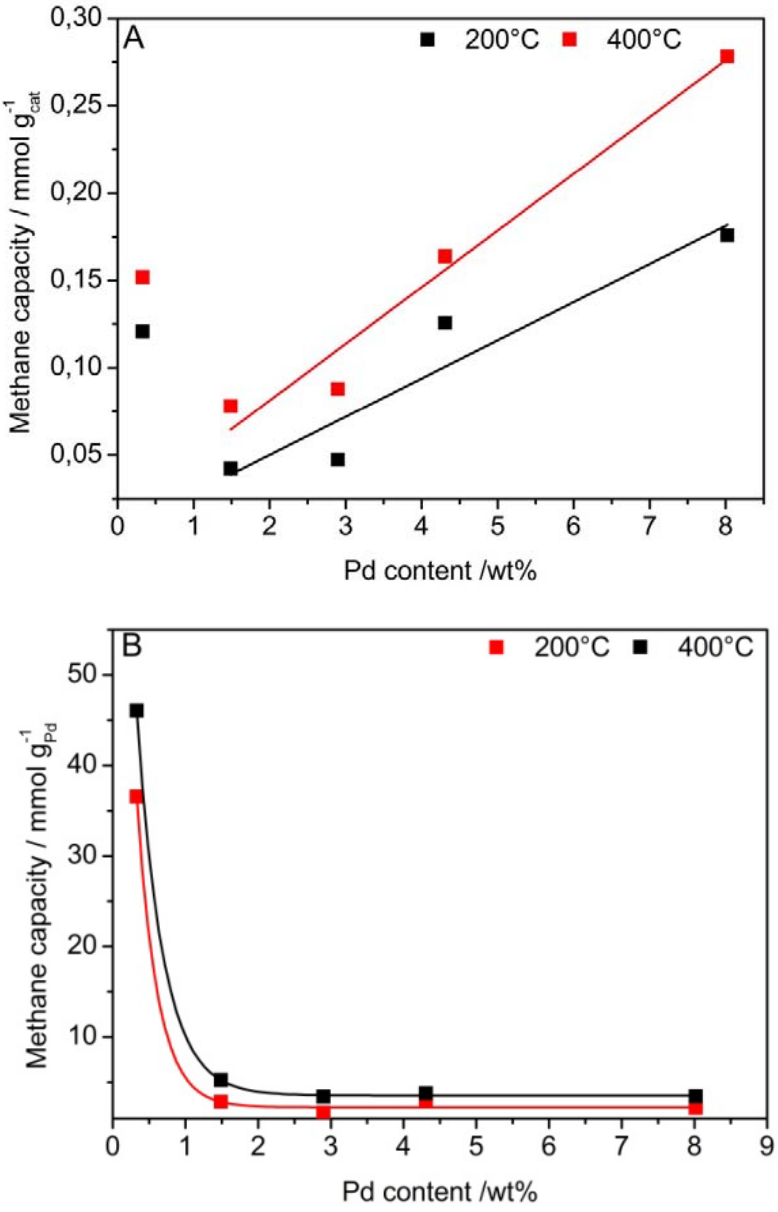

Figure 11: Methane capacity per gram catalyst (A) and per gram Pd (B).

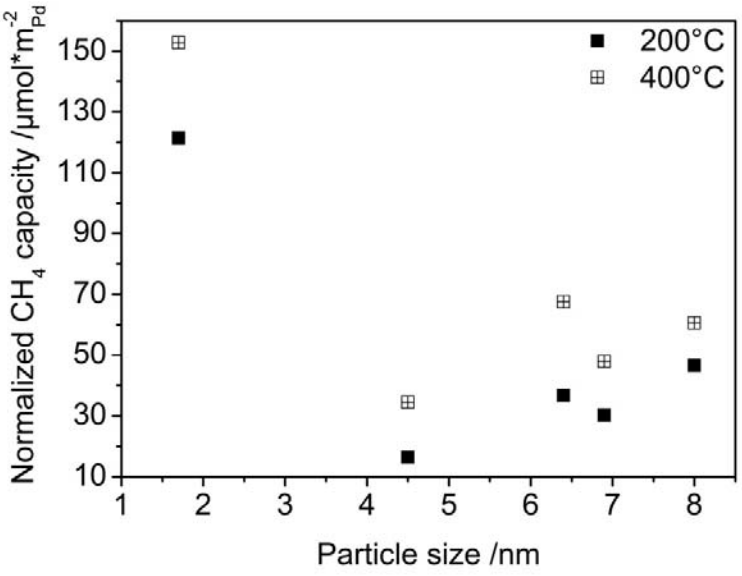

Figure 12: Correlation between Pd dispersion determined by CO chemisorption and activity of methane adsorption at 200 and 400 °C.

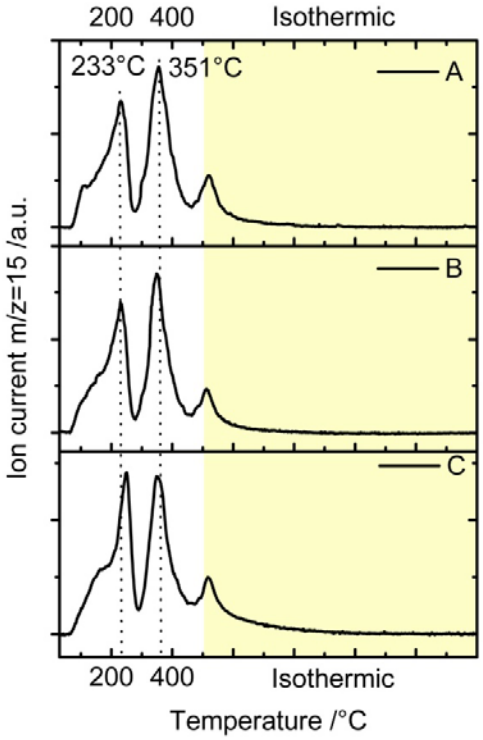

Figure 13: A- 1st TPSH at 400 °C after reduction; B- 2nd TPSH at 400 °C after TPSH1 + reduction; C- 3rd TPSH after oxidative and reductive treatment at 500 °C.

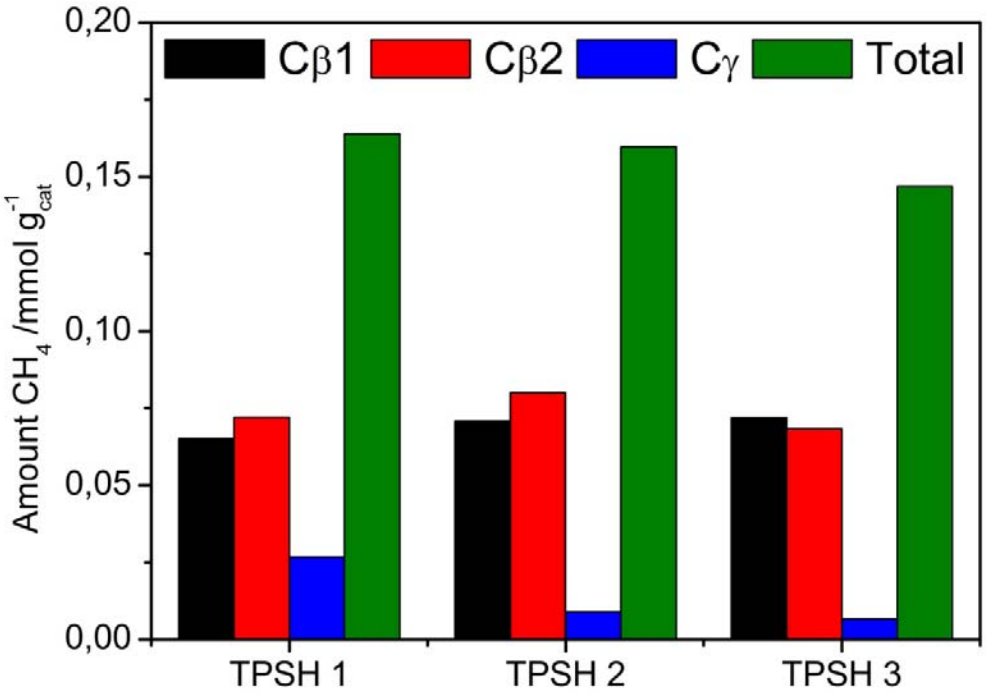

Figure 14: Quantitative methane formation during consecutive adsorption-hydrogenation cycles of catalyst Pd15.

Table 1: Composition, lattice parameter and surface area of the HTl samples.

Sample name	Pd:Mg:Al ratio	Lattice parameter		SA Precursor [m²/g]	SA after reduction at 500 °C [m²/g]
		a [Å]	c [Å]		
Pd0	0.0:60.9:39.1	3.032	22.759	191	196
Pd01	0.1:60.6:39.3	3.032	22.769	134	242
Pd05	0.6:60.4:39.0	3.034	22.866	126	231
Pd10	1.1:62.4:36.5	3.032	22.904	146	219
Pd15	1.9:59.1:39.0	3.031	22.807	113	223
Pd25	3.5:67.0:29.5	3.052	23.038	84	202

Table 2: Particles sizes of the reduced samples determined by TEM and chemisorption.

Sample name	Pd content ex-HTlc [wt-%]	Particle size TEM [nm]	PS Vol weighted [nm]	Dispersion CO [%]	Particle size CO [nm]	IFR* [%]
Pd01	0.33	n.d.	n.d.	67	1.7	-
Pd05	1.49	1.9	2.1	17	6.4	78
Pd10	2.90	2.2	2.5	25	4.5	63
Pd15	4.31	3.5	4.5	14	8.0	64
Pd25	8.02	3.3	3.7	16	6.9	64

* Interface ratio = $SA_{Chemisorption}/SA_{TEM}$

Table 3: Quantification of methane after adsorption at 200° and 400 °C.

Sample	Amount of CH_4 [µmol/g_{cat}] T = 200 °C				Amount of CH_4 [µmol/g_{cat}] T = 400 °C			
	$C_{\beta 1}$	$C_{\beta 2}$	C_{γ}	**Total**	$C_{\beta 1}$	$C_{\beta 2}$	C_{γ}	**Total**
Pd01	13.5	72.0	35.2	**120.7**	20.8	123.6	7.6	**152.0**
Pd05	12.4	25.4	4.5	**42.3**	14.4	53.6	10.0	**78.0**
Pd10	12.5	32.6	2.3	**47.4**	21.8	59.7	6.4	**87.9**
Pd15	71.9	47.7	6.1	**125.7**	65.1	72.0	26.7	**163.8**
Pd25	116.3	57.7	1.8	**175.8**	121.6	138.0	18.6	**278.2**

Supplementary Information

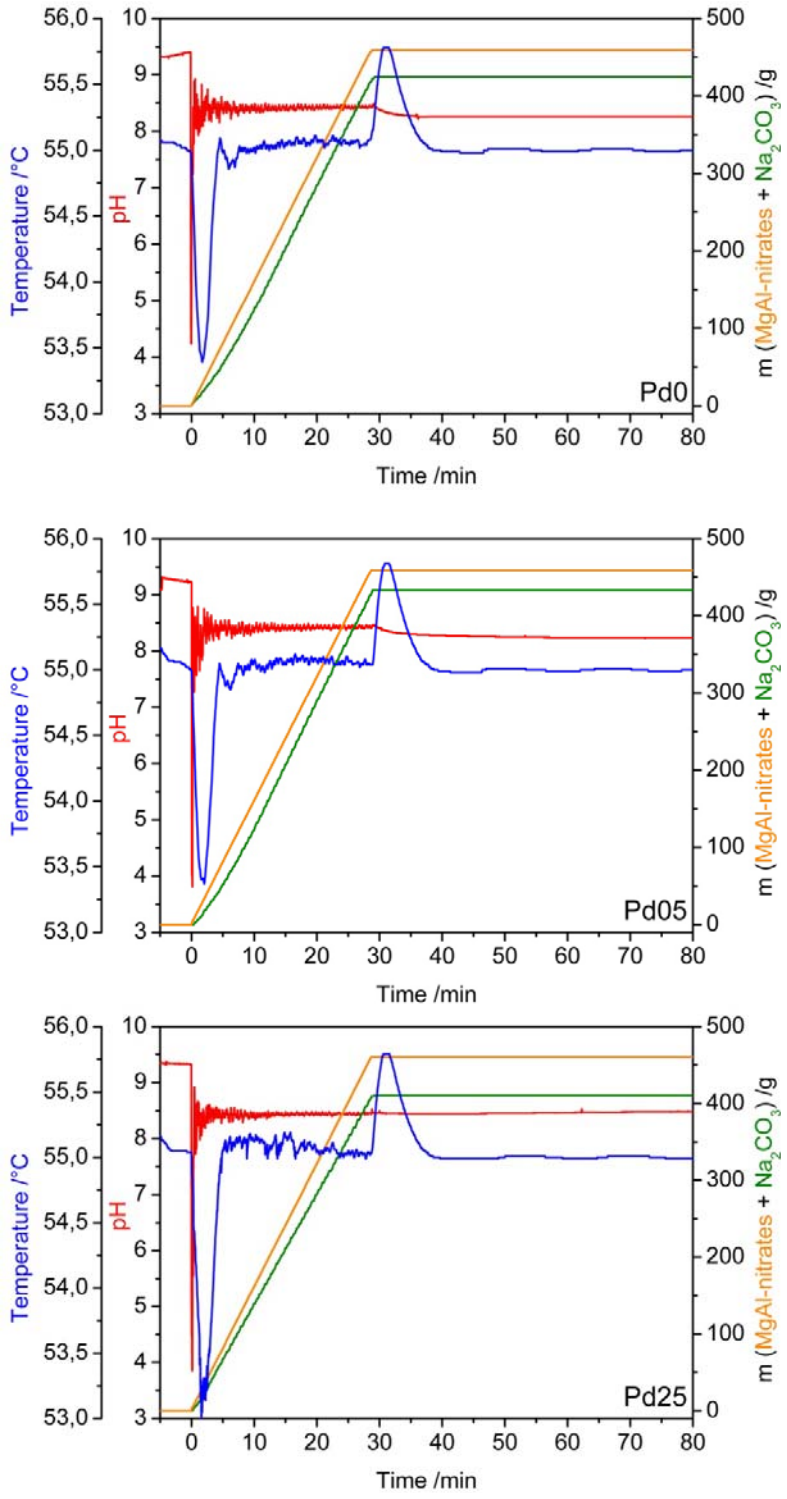

S 1: LabMax synthesis protocols of Pd0, Pd05 and Pd25.

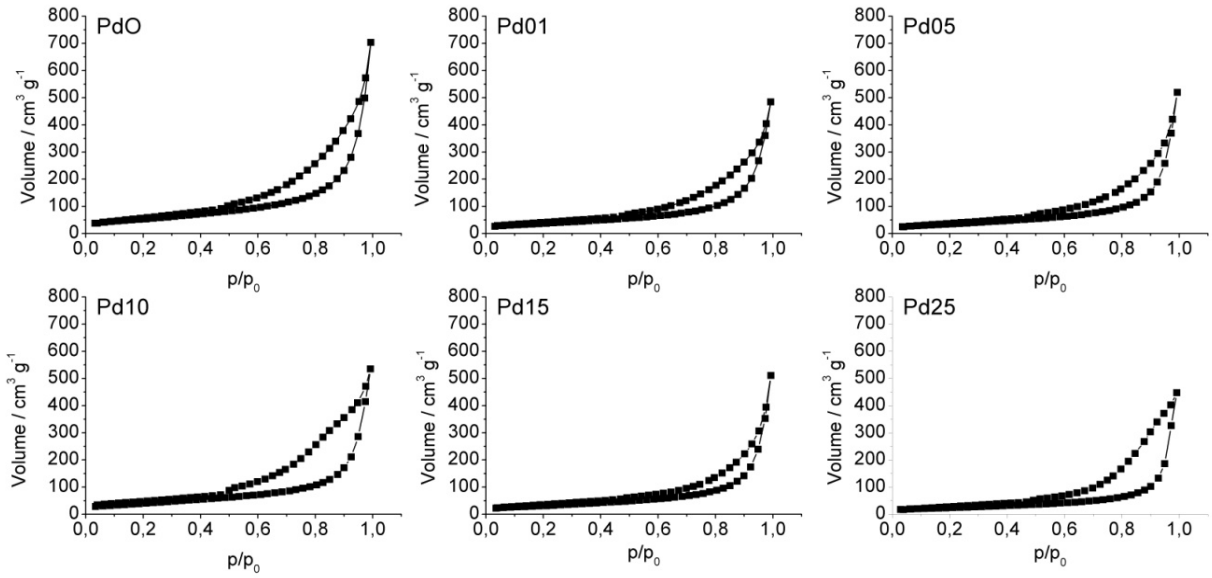

S 2: Nitrogen adsorption-desorption isotherm measured at -196 °C.

According to IUPAC (International Union of Pure and Applied Chemistry), the isotherm of undoped and doped samples is a type IV isotherm, which is typical for mesoporous materials. Characteristic for these samples is the presence of the hysteresis loop, which is associated with the occurrence of pore condensation. Also according to IUPAC classification, is characterized by a type H_2 hysteresis which can be associated a disordered pore structure. Considering the platelet-like morphology observed by SEM, HTl compounds are not characterized by pores but by spaces between the platelets where multilayer adsorption and, finally, “pore” filling can occur.